



HAL
open science

Experimental characterization of leading edge cracking on bulk tungsten divertor components during 2017–2019 WEST operation

M. Diez, J. Demiane, P. Reilhac, M. Lemetais, D. Dorow-Gerspach, J. Gerardin, J. Gaspar, C. Martin, A. Durif, M. Wirtz, et al.

► To cite this version:

M. Diez, J. Demiane, P. Reilhac, M. Lemetais, D. Dorow-Gerspach, et al.. Experimental characterization of leading edge cracking on bulk tungsten divertor components during 2017–2019 WEST operation. *Nuclear Materials and Energy*, 2024, 41, pp.101746. 10.1016/j.nme.2024.101746 . cea-04765326

HAL Id: cea-04765326

<https://cea.hal.science/cea-04765326v1>

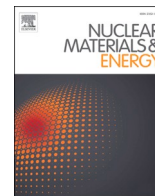
Submitted on 4 Nov 2024

HAL is a multi-disciplinary open access archive for the deposit and dissemination of scientific research documents, whether they are published or not. The documents may come from teaching and research institutions in France or abroad, or from public or private research centers.

L'archive ouverte pluridisciplinaire **HAL**, est destinée au dépôt et à la diffusion de documents scientifiques de niveau recherche, publiés ou non, émanant des établissements d'enseignement et de recherche français ou étrangers, des laboratoires publics ou privés.



Distributed under a Creative Commons Attribution 4.0 International License



Experimental characterization of leading edge cracking on bulk tungsten divertor components during 2017–2019 WEST operation

M. Diez^a, J. Demiane^a, P. Reilhac^a, D. Dorow-Gerspach^b, M. Lemetais^c, J. Gerardin^a, J. Gaspar^d, C. Martin^e, A. Durif^a, M. Wirtz^b, T. Loewenhoff^b, the WEST team¹

^a IRFM, CEA, Saint-Paul-Lez-Durance 13108, France

^b Forschungszentrum Jülich GmbH, Institut für Energie- und Klimaforschung - Plasmaphysik, Jülich 52425, Germany

^c Mines Saint Etienne, CNRS UMR 5307 LGF, Centre SMS, St Etienne F-42023, France

^d CNRS, IUSTI, Aix Marseille University, Marseille 13013, France

^e PIIM, CNRS, Aix Marseille University, Marseille 13013, France

ARTICLE INFO

Keywords:

Cracks
WEST
Tungsten
Depth
Length
Density

ABSTRACT

During the 2017–2019 WEST operation, a set of ITER-like plasma-facing units consisting of tungsten monoblocks was installed on the lower divertor. Despite modest heating power, 27 % of these monoblocks had cracks on their poloidal leading edges, which were not protected by a toroidal bevel. A comprehensive experimental characterization of the 133 cracked monoblocks indicates that damage occurs near the plasma strike point areas where neat cracks separated by 0.15–0.5 mm in the poloidal direction were observed. Cracks are up to 1 mm long and 1 mm deep and did not affect the lower divertor ability to sustain long pulses. The most important parameter affecting crack formation is the relative vertical misalignment between components.

Introduction

During its first phase of operation, WEST has operated with a set of actively-cooled ITER-like plasma facing units (PFUs) prototypes on one of the lower divertor sectors, called divertor test sector. These prototypes are using the tungsten monoblock technology and were delivered by six different suppliers from China, Japan and Europe (F4E), each having their own manufacturing processes.

Visual inspections of the divertor test sector in the course of 2017–2019 revealed surprising crack formations on these PFUs [1,2,3]. Depending on the degree of damage, cracking may have significant impact on the lifetime and reliability of the divertor. Cracking can be induced by different parameters: the impact of the plasma on the PFUs (during steady state or transient events), the PFUs assembly procedure (relative vertical misalignment) or/and the PFUs features related to their fabrication and design (W grade, toroidal bevel, surface machining, chamfers on the poloidal edges, thermo-mechanical treatments affecting the W microstructure, etc).

Because of this wide range of parameters that may be inter-related, the mechanism of W cracking in a tokamak environment is not yet well understood. Yet it is crucial to understand the cause of crack initiation and propagation to better avoid them in future tokamaks like

ITER, emphasizing the need to characterize these cracks.

Therefore, in this paper we provide an experimental characterization of the cracks formed on the leading edges of non-beveled ITER-like PFUs in WEST during the 2017–2019 period in order to better see the impact of certain parameters on the cracking response. This exhaustive characterization aims in particular to assess the impact of chamfering on crack formation, the differences between the inner strike point (ISP) and outer strike point (OSP), the impact of vertical misalignment of the components on their level of damage as well as to detect any differences in behavior due to manufacturing choices.

Materials and method

Materials

Between 2017 and 2019, WEST had run 4 experimental plasma campaigns referred to as C1 to C4. While C1 and C2 were devoted to developing plasma scenario, C3 and C4 experienced more particle and power loads. During that same period, ITER-like PFUs (ILP) made of 35 tungsten monoblocks (MBs) each were progressively installed on the test divertor sector. The ILPs were not toroidally bevel (flat top geometry) as foreseen in ITER. In this paper, chamfering refers to the 1x1mm chamfer

¹ See <http://west.cea.fr/WESTteam>.

that some PFUs had on both their leading and trailing edges.

During the C3 campaign (2018), 12 ILPs were installed on the lower divertor, including 2 PFUs with unchamfered poloidal edges. They were exposed to the plasma for about 2 h (L mode operation, divertor peak heat flux $\sim 1\text{--}2.5\text{ MW/m}^2$ at the outer strike point, leading to an estimate of parallel heat flux of $\sim 40\text{--}50\text{ MW/m}^2$) but experienced a significant number of transient events (~ 700 disruptions).

During the C4 campaign (2019), 2 ILPs with unchamfered poloidal edges were added to the sector, leading to a total of 14 PFUs. Between C3 and C4, the toroidal position of some ILPs changed to meet the needs of the experimental program. They were exposed to about 3.5 h (L mode operation, divertor peak heat flux $\sim 6\text{ MW/m}^2$, leading to an estimate of parallel heat flux of $\sim 70\text{--}90\text{ MW/m}^2$).

In this paper, PFUs are identified as ILPi in reference to their toroidal position. More details on PFU identification and their toroidal position for each campaign can be found in [1].

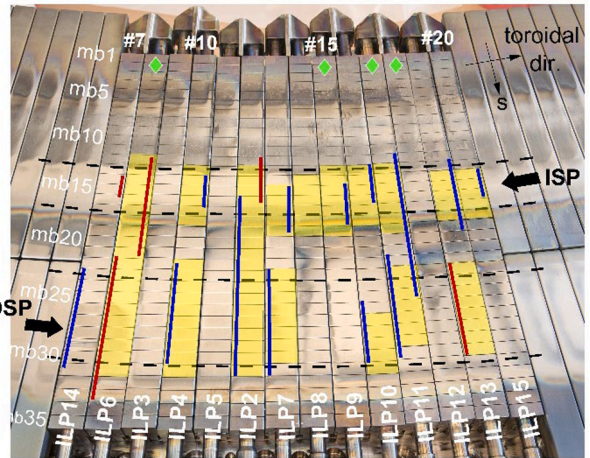
An infrared (IR) camera is positioned above the test divertor sector to monitor the surface temperature of monoblocks [4]. However, due to its limited field of view (a few monoblocks), it does not allow global monitoring. It is mainly used to monitor components dedicated to specific experiments [5,6], limiting the IR analysis in this paper.

Method

After the C3 and C4 shutdown, the ITER-like PFUs dismantled and removed from the divertor were systematically observed using a DINO-LITE digital microscope to determine their state of damage. This was used to determine the number of components/monoblocks showing cracks on the leading edge, as well as the location of the cracks in relation to the configuration of the test divertor sector. After C1/C2, no PFUs could be observed but 5 PFUs and 13 PFUs were available for observation after C3 and C4, respectively.

An in-depth analysis using chromatic confocal microscopy (STIL [7]) was then carried out of all available cracked PFUs to evaluate the average crack length and density. In total, 133 monoblocks were analysed by confocal microscopy (identified in yellow in Fig. 2). To optimize the process, the analysis was carried out on the top surface of the monoblocks only and measurements were taken at the center of the leading edges of the monoblocks, with dimensions of $7 \times 2\text{ mm}^2$ (see Fig. 1a). Resolution in the toroidal direction was $4\text{ }\mu\text{m}$ and $2.5\text{ }\mu\text{m}$ in the 's' direction. Acquisition frequency was 300 Hz.

The acquired image was then directly analyzed using ImageJ software coupled to the Kappa 'curvature analysis' plugin. Cracks were identified by the software based on the image contrast. Using the



- ◆ unchamfered ITER-like PFUs
- cracks observed after C3 without evolution after C4
- cracks observed after C4
- monoblocks analyzed by confocal microscopy for crack length and density

Fig. 2. Photograph of the lower divertor sector after the 2019 campaign (c4) showing the location and the number of monoblocks with cracks on their leading edges.

number of pixel and a calibrated scale, the software calculates the length of each crack and thus an average crack length can be given for each monoblock. The crack density was determined by calculating the number of identified cracks and dividing it by the scanned length along the 's' coordinate. This allowed to express the crack density as cracks per millimetre. An example describing the data analysis process for ILP4 MB16 is given in Fig. 1b,c.

Finally, a number of the cracked PFUs/monoblocks were cut into small samples and examined using optical microscopy (PRESI, HZ30-4) and scanning electronic microscopy (SEM) (ZEISS Evo Ma10 and ZEISS DSM 982 Gemini) to assess the morphological features of the cracks.

A metallographic analysis was also performed on chamfered ILP7 and unchamfered ILP6 to evaluate the crack depth as these cracks could have a significant impact on the components ability to extract heat. In the case of the chamfered component, the entire width of MB27 was examined by successive grinding steps up to 2 mm into the leading edge (see Fig. 5) in order to get a global insight and solid statistics of the crack

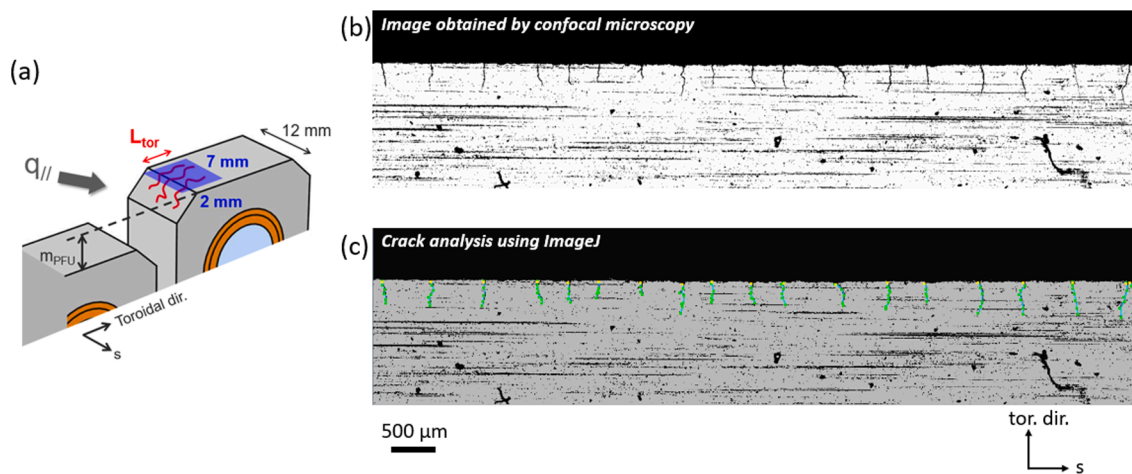


Fig. 1. (a) schematic illustration showing the $7 \times 2\text{ mm}^2$ area on the leading edge where the crack analysis was performed. (b) image obtained by confocal microscopy, here in the case of MB16 ILP4. (c) This image is then analyzed by ImageJ which identifies each crack and calculates its length and density. Here the average crack length was $231\text{ }\mu\text{m}$ and the crack density was $2.71\text{ }\mu\text{m}$ for MB16 ILP4.

depth distribution along the MB width and as a function of the distance from the leading edge.

Results

Visual inspection

Fig. 2 shows the configuration of the test divertor sector during the C4 campaign (2019). The 14 ITER-like PFUs installed in toroidal position from 7 to 20 are visible with their ILPi identification. Unchamfered PFUs are indicated by green diamonds, while the location of the inner striking point (ISP) and the outer striking point (OSP) is indicated by black dotted lines.

Microscope observations at the end of C4 revealed that 10 out of the 14 PFUs had cracks on their poloidal edges. Cracks on ILP14 (ISP), ILP6, ILP2 (ISP), ILP13 (OSP) were observed during the shutdown following the C3 campaign and are therefore attributed to C3. On the other hand, cracks on ILP14 (OSP), ILP4, ILP2 (OSP), ILP7, ILP9, ILP10, ILP11, ILP13 (ISP) and ILP15 are believed to have formed during C4. ILP3, ILP5 and ILP8 did not reveal cracks at the end of C4 because their leading edges were not exposed to the plasma (negative vertical misalignment). Similarly, ILP9 and ILP15 had no cracks in the OSP because their leading edges were negatively misaligned (shadowed by their upstream neighbors). There are no data associated with unchamfered ILP12 because it was not available for the characterization program.

In total, it represents 133 monoblocks with cracks, or 27 % of the monoblocks. The cracks are located on the leading edges of the monoblocks, mainly around the inner and outer strike point areas where plasma heat load is the highest.

Some cracks are also visible on the private flux region (MB19-23) and sometimes on the trailing edges. Unchamfered PFUs show the same behavior in terms of number and location of damaged monoblocks as the chamfered PFUs.

Observation at low magnification

Fig. 3 shows the topography of the leading edge of 3 cracked MBs located in the OSP region, coming from unchamfered ILP11, chamfered ILP13 and chamfered ILP7. The cracks are visible on the top surface of the MBs propagating in the toroidal direction as well as on their poloidal side surfaces. On ILP11 and ILP13, the cracks are neat and quite regularly spaced in the 's' direction. The cracks therefore appear identical on components provided by 2 different manufacturers, independently of the presence or absence of a 1mmx1mm chamfer on the leading edges. Sometimes, but not all the time, there is an alternation of long crack, then short, then long, reminiscent of EAST's proposal for the crack formation process (primary/secondary crack) [8], though never clearly established in WEST.

Chamfered ILP7 was found to be damaged in a different way to the

other components. Numerous interconnected cracks resembling a crack network are visible on the chamfer and top surface, extending several mm in the toroidal direction. To verify this result, MB35 of the same PFU was also observed. A network of micro-cracks was observed on the top surface, despite the fact that this monoblock does not see plasma in the WEST configuration. This suggests that micro-cracks were initiated during the fabrication of the component and then developed during plasma exposure. A comparative metallographic analysis should be carried out on components from different manufacturers to confirm this result.

The photos in Fig. 3 are from observations made after the C4 campaign, but it should be noted that several components were observed after C3 and again after C4, when possible. The PFUs with cracks after C3 and still misaligned during C4 do not show any crack propagation or additional cracks (see Fig. 9 of [9]), suggesting that the cracks are quite stable once they formed.

Observation at high magnification

At higher magnification the cracks appear to be discontinuous as illustrated on Fig. 4a. The long cracks observed at low magnification are sometimes the alignment of several small cracks, which do not seem to be connected to each other. At the leading edge, where the crack is most open, crack width was measured around 5–15 μm . Another interesting feature of these cracks is the presence of beads of material on both sides of the crack groove (Fig. 4b). These bumps are observed for almost all cracks, in the OSP region but also in the ISP region, for both unchamfered and chamfered PFUs. No further characterization has been carried out to understand the formation of these material's beads (molten edges? material deformation during crack opening?). They therefore remain an open question today.

Metallographic examination

In order to determine the depth of the cracks, and consequently, their potential impact on the component's heat exhaust capability, a metallographic analysis was performed on the two most damaged PFUs (ILP7 and ILP6) on OSP-located MBs.

Fig. 5a shows the results obtained for chamfered ILP7 on MB27, which was vertically misaligned by 0.3 mm with respect to its upstream neighbour during C4. The leading edge was progressively grinded and polished up to 2 mm in 5 examination steps, corresponding to examination layers L1 to L5. The crack depth distribution is quite broad, ranging from practically zero to the deepest of around 350 μm on this monoblock. Inside the chamfer, an average crack depth of about 50 μm was measured. Cracks are deepest at the edge of the chamfer, averaging up to 130 μm . Then, as going deeper into the material, the cracks become shallower and shallower, with an average of about 30 μm at 2 mm from the leading edge.

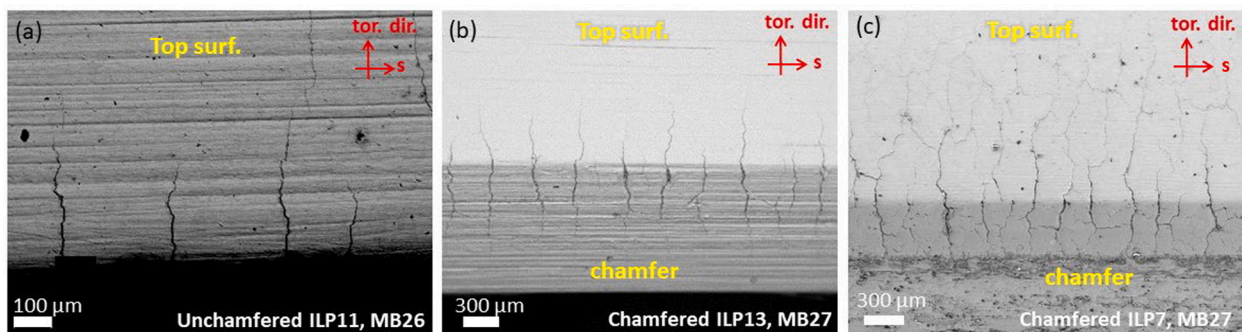


Fig. 3. SEM images revealing the topography of cracked monoblocks observed on the leading edge in the OSP region (a) MB26 unchamfered ILP11 (b) MB27 chamfered ILP13, (c) MB27 chamfered ILP7.

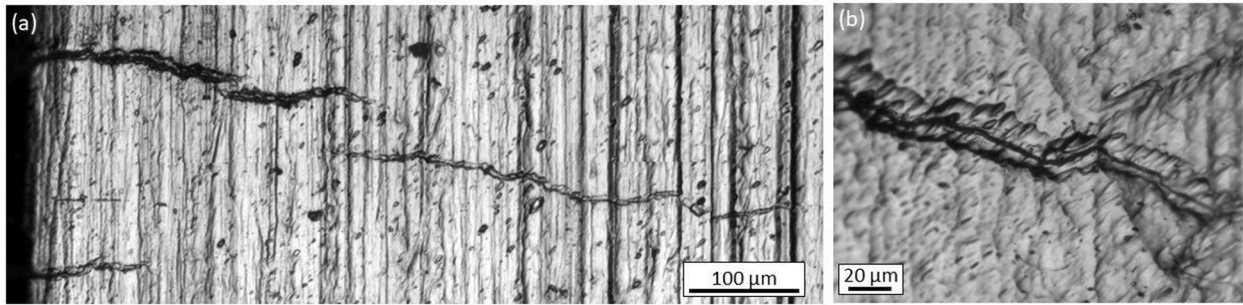


Fig. 4. Optical microscope images showing the cracks features on the top surface of unchamfered (a) ilp11, mb27 and (b) ilp13 mb27.

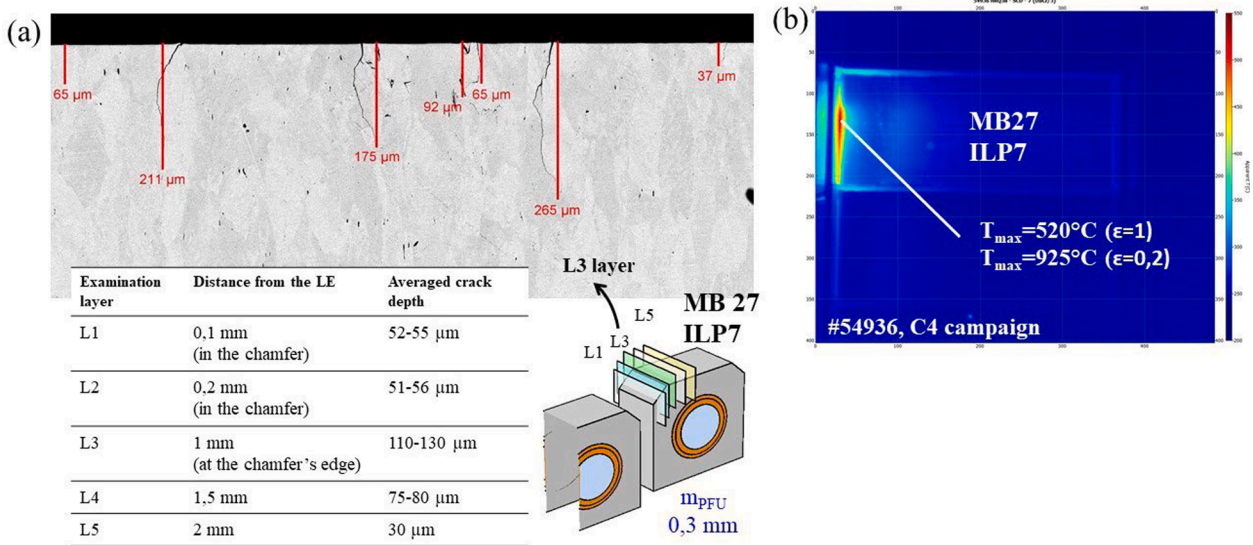


Fig. 5. (a) optical microscopy image showing the crack depth at the edge of the chamfer (examination layer L3) of MB27 ILP7. The table shows the averaged crack depth measured for each examination plan. (b) IR image of the same MB during shot#54936 at t = 12 s when thermal equilibrium is reached.

Although it is difficult to link post-mortem observations to a specific plasma event, infrared cameras can be a good tool when discussing damage to monoblock surfaces [10]. An IR image taken during the C4 campaign (Fig. 5b) (shot#54936, $P_{inj} = 3.5-4.0$ MW, stationary heat flux for at least 6 s, estimated parallel heat flux $70-90$ MW/m²) shows that the monoblock surface can reach $500-900$ °C (depending on emissivity), above the ductile-to-brittle transition temperature.

The other component is ILP6, for which cracks were observed after C3 both in the ISP and OSP areas [2]. During C3 this component was highly misaligned (+0.8 mm) and an IR image taken during C3 (Fig. 6b) indicate that the surface temperature of MB27 reached $800-1000$ °C (depending on emissivity) in steady state. A modest parallel heat flux

was estimated at $40-50$ MW/m², which is unlikely to have generated cracks. At that stage, no microstructure observation could be made. The only metallographic analysis was performed after C4 on MB24 (see Fig. 6a). It can be seen that damage is more severe than for the previous MB. A different crack structure is observed, with the presence of cracks parallel to the surface and much longer cracks, measured up to about 1.1 mm. It is also clear that recrystallization of tungsten occurred near the surface. Independently of the cause of recrystallization, the damage is more severe. This difference in damage could be the direct consequences of W recrystallization (degradation in materials properties such as a loss of mechanical strength, fracture toughness and embrittlement) or could be the result of a different initial microstructure of W.

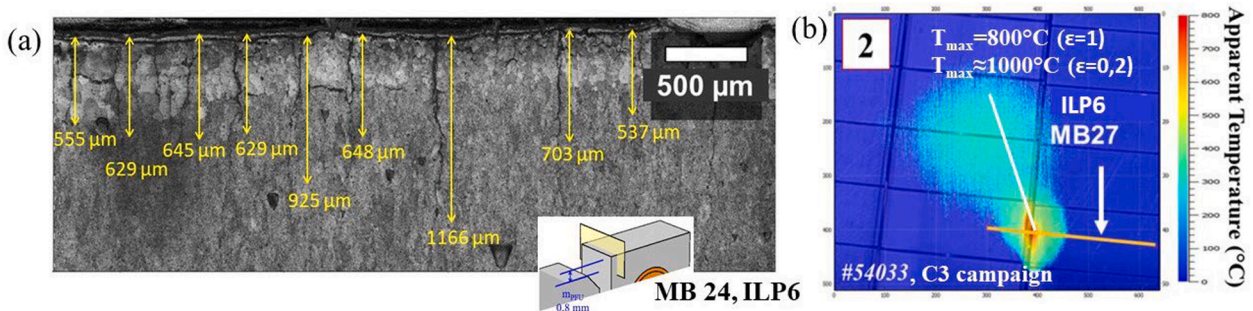


Fig. 6. (a) Optical microscopy image showing the state of damage of the leading edge of MB24 ILP6 after C4 (surface polished over 300 μm). (b) IR image of ILP6 MB27 during shot#54033. The image is taken from [11].

Crack length and density

An extensive characterization of all 133 cracked monoblocks enabled us to determine the average length and linear density (number of cracks / mm) of the cracks on each monoblock. Fig. 7 shows that cracks in the OSP region are twice as long as those in the ISP region, with lengths ranging from 0 to 1000 μm in the OSP region and 0 to 500 μm in the ISP region. It should be noted that these values are averages, meaning that cracks can be longer than 1000 μm in some cases. Furthermore, as mentioned in the previous paragraph, cracks are discontinuous and length measurement can therefore be tricky, but this does not change the trend for longer cracks in OSP than in ISP. No difference is observed between chamfered MBs (circular markers) and unchamfered MBs (star markers). As damage is generally related to heat flux, the fact that cracks are more severe in the OSP than in the ISP seems unsurprising due to the in/out asymmetry observed in many tokamaks, which gives rise to higher heat fluxes in the OSP than in the ISP.

The figure also shows the positions of the strike points (SP) during C3 and C4. In the OSP region, the strike point was often positioned very locally on MB24, or even MB25, where the heat flux is supposed to be higher. However, cracks are present over a very wide area from MB22 to MB31. For example, MB30 exhibits cracks up to 300 μm long, despite being located far from the SP zone, where intense steady state heat loads are not expected. Even with the assumption that the peak heat flux shifts 1 or 2 MBs away from the SP, the figure shows that cracking occurred in regions where it was not expected. Such significant damage far from the strike point region reinforces the hypothesis of previous research that disruptions could have a big role to play in cracking mechanisms [2,3,12].

Fig. 8 shows the crack density for each monoblock, i.e. the number of cracks per mm. It is between 2 and 6, i.e. each crack is separated by 0.15 to 0.5 mm in the poloidal direction, whether the monoblock is chamfered or not. It therefore appears that once formed and stable, the cracks have a regular spacing which seems to be an intrinsic behavior of W.

Impact of vertical misalignment

It was then intended to see the variation of the average crack length with respect to the vertical misalignment of the PFUs (Fig. 9). For the cracks believed to have formed during C3, the value of the misalignment of the PFUs during C3 was taken. Otherwise, the misalignment data

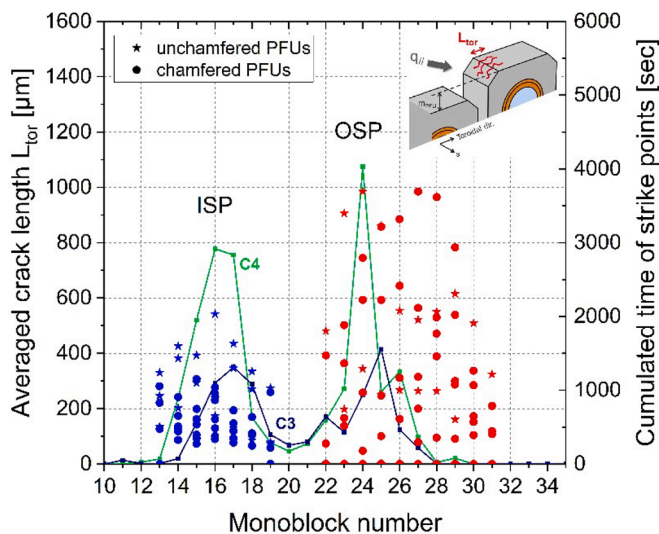


Fig. 7. Average crack length in the toroidal direction, combined with the position of the strike points during the c3/2018 (blue line) and c4/2019 (green line) campaigns. (For interpretation of the references to colour in this figure legend, the reader is referred to the web version of this article.)

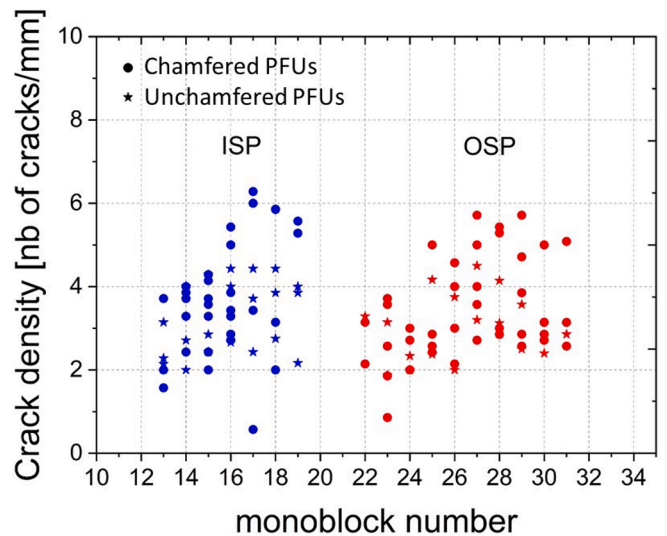


Fig. 8. Crack density for each of the cracked monoblock.

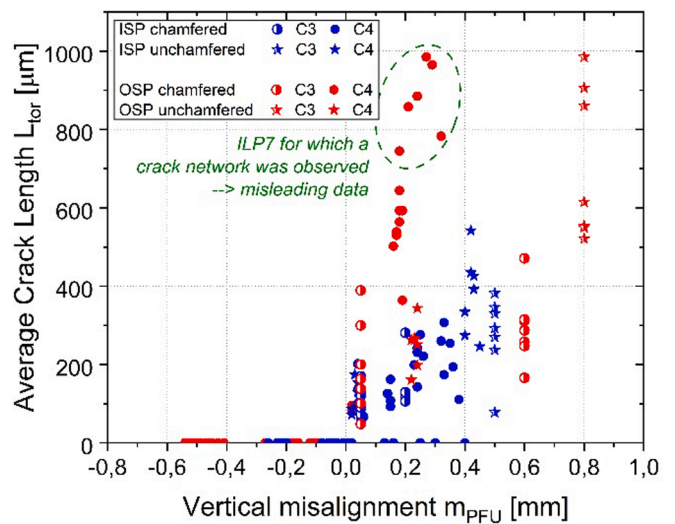


Fig. 9. Measured average crack length versus relative vertical misalignment.

pertains to the C4 campaign. The data points circled in green belong to ILP7, for which a crack network was observed on the leading edge. Compared to the other PFUs with neat cracks (see 3.2), the measurement of the crack length is therefore much more difficult for this PFU and might be inaccurate.

The figure clearly shows that positive misalignment necessarily leads to cracking, as all non-cracked MBs are associated with negative misalignment. With the non-beveled geometry of the MB, the leading edges are not protected, so vertical misalignment plays an important role. Today, there are no alignment tolerances for these non-beveled components (existing tolerances only apply to beveled PFUs), but it can be seen that a misalignment of 0.1–0.2 mm can already result in cracks > 200 μm . The higher the misalignment the longer the cracks.

Conclusion

Cracking of ITER-type PFUs during WEST operation between 2017–2019 was investigated experimentally through visual observations, confocal microscope measurements and metallographic examinations.

The results indicate that 27 % of all monoblocks had cracks on their

leading edges. The cracks are visible on both the poloidal side surface and the top surface, propagating up to about 1 mm in the toroidal direction. The cracks are neat but discontinuous, with material's bead on the sides on the crack groove.

One PFU exhibits a different cracking structure, with the presence of a crack network rather than neat cracks. As this component has not been exposed differently to the plasma than the others, manufacturing (choice of W material/microstructure, surface machining, etc) could be the main responsible of this cracking response but a comparative study between the different manufacturers would be necessary to confirm this assumption.

With the flat top geometry, the leading edges are not protected and a chamfer of 1mmx1mm on them is not sufficient to mitigate damage, as cracks were observed on chamfered poloidal leading edges, as well as on unchamfered leading edges. Any positive misalignment leads to cracking, and cracks tend to be longer in the toroidal direction when the misalignment is larger. As for the crack depth, it can vary from < 150 µm to 1 mm, depending on the component's alignment configuration, the presence or absence of a chamfer and the intensity of the heat flux to which it is exposed.

In WEST, cracking of the monoblocks was evidenced as early as the 2018 campaign, although the peak heat flux reached was relatively modest (2.5 MW/m² on top surface) and the surface temperature of the most misaligned monoblocks did not exceed 1000 °C in steady state. This suggests that much more intense and violent events, such as disruptions, could have damaged the leading edges of the monoblocks. This is all the more true as monoblocks far from the strike points, where almost no heat flux is expected in permanent regime, also cracked. However, it should not be forgotten that recrystallization can also degrade the material and lead to premature cracking of the W, or at least make the damage more severe, as observed in this paper.

Although further studies would be needed to better understand the mechanisms behind crack formation, it is evident that a toroidal bevel should be applied to the monoblocks to avoid any risk of damage on the LE during operation. This design is foreseen in ITER and is currently being tested with the lower divertor targets installed in WEST since 2021. So far, no cracks on the LE have been observed.

CRedit authorship contribution statement

M. Diez: Writing – original draft, Methodology, Investigation. **J.**

Demiane: Writing – review & editing, Investigation. **P. Reilhac:** Investigation. **D. Dorow-Gerspach:** Writing – review & editing, Investigation. **M. Lemetais:** . **J. Gerardin:** Investigation. **J. Gaspar:** Investigation. **C. Martin:** Writing – review & editing, Investigation. **A. Durif:** Investigation. **M. Wirtz:** Investigation. **T. Loewenhoff:** Investigation.

Declaration of competing interest

The authors declare that they have no known competing financial interests or personal relationships that could have appeared to influence the work reported in this paper.

Data availability

Data will be made available on request.

Acknowledgments

This work has been carried out within the framework of the EUROfusion Consortium, funded by the European Union via the Euratom Research and Training Programme (Grant Agreement No 101052200 — EUROfusion). Views and opinions expressed are however those of the author(s) only and do not necessarily reflect those of the European Union or the European Commission. Neither the European Union nor the European Commission can be held responsible for them.

References

- [1] M. Diez, et al., *Nuclear Mater. Energy* 34 (2023) 101399.
- [2] J.P. Gunn, et al., *Nuclear Mater. Energy* 27 (2021) 100920.
- [3] Y. Corre, et al., *Nuclear Mater. Energy* 37 (2023) 101546.
- [4] M. Houry, et al., *Fusion Eng. Des.* 146 (2019) 1104–1107.
- [5] A. Grosjean, et al., *Nucl. Mater. Energy* 27 (2021) 100910.
- [6] Y. Corre, et al., *Phys. Scr.* 96 (2021) 124057.
- [7] E. Gautier, et al., *J. Nucl. Mater.* 438 (2013) S1216.
- [8] D. Zhu, et al., *Nucl. Fusion* 62 (2022) 056004.
- [9] M. Diez, et al., *Nucl. Fusion* 61 (2021) 106011.
- [10] Q. Tichit, et al., *Nuclear Mater. Energy* 37 (2023) 101537.
- [11] A. Grosjean, et al., *Nucl. Fusion* 60 (2020) 106020.
- [12] A. Durif, et al., *Fusion Eng. Des.* 188 (2023) 113441.